

Probing the Strong Nonadiabatic Interactions in the Triazolyl Radical Using Photodetachment Spectroscopy and Resonant Photoelectron Imaging of Cryogenically Cooled Anions

Yue-Rou Zhang, Dao-Fu Yuan,* and Lai-Sheng Wang*



Cite This: *J. Am. Chem. Soc.* 2022, 144, 16620–16630



Read Online

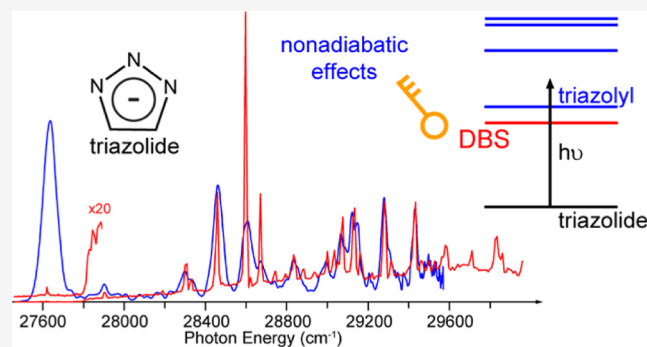
ACCESS |

Metrics & More

Article Recommendations

Supporting Information

ABSTRACT: Although the adiabatic potential energy surfaces defined by the Born-Oppenheimer approximation are the cornerstones for understanding the electronic structure and spectroscopy of molecular systems, nonadiabatic effects due to the coupling of electronic states by nuclear motions are common in complex molecular systems. The nonadiabatic effects were so strong in the 1,2,3-triazolyl radical ($C_2H_2N_3$) that the photoelectron spectrum of the triazolide anion was rendered unassignable and could only be understood using nonadiabatic calculations, involving the four low-lying electronic states of triazolyl. Using photodetachment spectroscopy and resonant photoelectron imaging of cryogenically cooled anions, we are able to completely unravel the complex vibronic levels of the triazolyl radical. Photodetachment spectroscopy reveals a dipole-bound state for the triazolide anion at 172 cm^{-1} below the detachment threshold and 32 vibrational Feshbach resonances. Resonant photoelectron imaging is conducted by tuning the detachment laser to each of the Feshbach resonances. Combining the photodetachment spectrum and the resonant photoelectron spectra, we are able to assign all 28 vibronic peaks resolved for the triazolyl radical. Fundamental frequencies for 12 vibrational modes of the ground state of the triazolyl radical are measured experimentally. The current study provides unprecedented experimental vibronic information, which will be valuable to verify theoretical models to treat nonadiabatic effects involving multiple electronic states.



1. INTRODUCTION

The separation of nuclear and electronic motions defined by the Born–Oppenheimer approximation gives rise to adiabatic potential energy surfaces, which form the foundation to understand the electronic structure and spectroscopy of molecular systems. Vibrational spectroscopy and many chemical processes can be analyzed on adiabatic potential energy surfaces, while photophysical processes can be understood as transitions between adiabatic potential energy surfaces. However, nonadiabatic processes, which represent a breakdown of the Born–Oppenheimer approximation, can occur in complex molecular systems due to the coupling of two or more adiabatic potential energy surfaces, in particular for electronic states which are energetically proximate.^{1–3} The Jahn–Teller effects and conical intersections are the most dramatic manifestation of the breakdown of the Born–Oppenheimer approximation and can profoundly influence and complicate electronic spectroscopies. Strong nonadiabatic effects have been observed in a series of azolyl radicals, five-membered carbon–nitrogen heterocycles,^{4–14} which are isoelectronic to the C_5H_5 cyclopentadienyl radical. The ground state of C_5H_5 is a $^2E''$ doubly degenerate state due to its partially filled π HOMO (e''^3), which undergoes static Jahn–

Teller distortion.^{15–17} Substitution of the CH groups with nitrogen atoms reduces the symmetries of the azolyls, resulting in conical intersections. Nitrogen-containing heterocycles are building blocks of biomolecules. The conical intersections are considered to be important for the photostability of biomolecules because UV absorption of these molecules is followed by ultrafast nonadiabatic relaxation from electronic excited states to the ground state *via* conical intersections.^{18–20}

Photoelectron spectroscopy (PES) of anions is a powerful technique to probe the low-lying electronic states of molecular systems and nonadiabatic effects. The Lineberger group reported PES studies of a number of azolide anions,^{4–8} providing a plethora of vibronic information for the azolyl radicals, including pyrrolyl, imidazolyl, pyrazolyl, and triazolyl. The PES data have revealed strong nonadiabatic effects and have been interpreted with sophisticated nonadiabatic vibronic

Received: July 7, 2022

Published: September 1, 2022



coupling calculations.^{8–14} It was found that the vibronic couplings became stronger with increasing numbers of N atoms because the N lone pairs give rise to additional low-lying electronic states in the azolyl radicals. Although the PES data could be understood using a two-state coupling model for pyrrolide and imidazolide,^{9,11} a three-state coupling model was necessary for pyrazolide.^{8,10} The vibronic coupling was so strong in triazolyl that Lineberger and co-workers could not make any assignments to the observed vibronic features in the PES data,⁷ which were only understood qualitatively by Yarkony and co-workers through spectral simulations using a quasidiabatic Hamiltonian comprising polynomials to the fourth order.^{12,13}

We have developed a high-resolution photoelectron imaging (PEI) apparatus coupled with an electrospray ionization (ESI) source and a cryogenically cooled ion trap.²¹ We have shown that both cold anions and high spectral resolution are essential to resolve fine vibronic structures in complex anions.^{22–26} More importantly, we have developed resonant PES (rPES) for polar anions that can support dipole-bound states (DBSs) *via* vibrational autodetachment,²⁷ which results in much richer spectroscopic information than conventional PES. DBSs in anions are analogous to Rydberg states in neutral molecules that have been used for developing high-resolution zero-kinetic energy (ZEKE) spectroscopy,^{28,29} in which neutral molecules are resonantly excited to high Rydberg states slightly below the ionization threshold of the molecules, followed by field ionization. In principle, Rydberg spectroscopy is more general and can be used for any neutral molecules, whereas DBSs can only exist in polar anions. However, the Rydberg spectroscopy can be very complicated due to the presence of multiple Rydberg states and has been applied to relatively simple molecules.^{28,29} A single DBS usually exists for polar anions, allowing relatively large anions to be investigated.^{30–33} Recently, we have initiated a series of studies to obtain high-resolution PES data for the azolide anions using high-resolution cryogenic ESI-PEI.^{34,35} It turned out that pyrrolide and imidazolide do not support DBSs because the dipole moments of the corresponding pyrrolyl and imidazolyl radicals are below the empirical critical value (~ 2.5 D).³⁶ Nevertheless, the high-resolution PEI data still yielded considerably more vibronic fine features and vibrational information.³⁴ Due to the large dipole moment of the pyrazolyl radical, we did observe DBSs for the pyrazolide anion. In fact, we even observed a core-excited DBS because the first excited state (\tilde{A}^2B_1) of pyrazolyl is only 266 cm^{-1} above its ground state (\tilde{X}^2A_2).³⁵

In the current study, we report a high-resolution PEI, photodetachment spectroscopy (PDS), and rPES study of cryogenically cooled triazolide anions. Fortunately, triazolide does support a DBS, allowing us to use the powerful PDS and rPES to unravel the complicated vibronic levels of the triazolyl radical. The cryogenic cooling eliminates all vibrational hot bands, which is critical for such a complicated vibronic system. Specifically, the similarity between the PDS and PES vibronic transitions has played a critical role in the spectral assignments. A DBS is observed at $172 \pm 7\text{ cm}^{-1}$ below the detachment threshold of triazolide, that is, the electron affinity (EA) of the triazolyl radical, at $3.4463 \pm 0.0009\text{ eV}$ ($27,796 \pm 7\text{ cm}^{-1}$). Thirty-one above-threshold vibrational Feshbach resonances are observed for the DBSs. Twenty-eight vibronic peaks are resolved in the spectral range $\sim 2000\text{ cm}^{-1}$ above the zero-point level of the triazolyl radical, and they are assigned by combining PDS, rPES, and the computed vibrational

frequencies. Fundamental vibrational frequencies for 12 vibrational modes of triazolyl (out of a total of 15 modes) are obtained experimentally. The current work provides unprecedentedly detailed vibronic information for the triazolyl radical, which will be important to calibrate more sophisticated multi-state vibronic coupling models to elucidate the non-adiabatic interactions in complex molecular systems.

2. EXPERIMENTAL METHODS

The experiments were carried out using our third-generation ESI-PES apparatus,²¹ equipped with a cryogenically cooled Paul trap²⁴ and a high-resolution PEI system.³⁷ The triazolide anions were generated by electrospray of a 1 mM solution of 1,2,3-triazole ($C_3H_3N_3$, Ambeed Inc.) in a CH_3OH/H_2O mixed solvent (9:1 volume ratio) spiked with several drops of NaOH to enhance deprotonation. The triazolide anions produced from the ESI source were guided into a cryogenically controlled Paul trap operated at 4.6 K and were cooled by collisions with a mixed He/ H_2 (4/1 volume ratio) buffer gas for 0.1 s before being pulsed into the extraction zone of a time-of-flight (TOF) mass spectrometer at a 10 Hz repetition rate. The triazolide anions were selected by a mass gate and allowed to enter the interaction zone of the VMI system, where they were crossed with a detachment laser beam from a dye laser or Nd:YAG laser. Photoelectrons were extracted and focused using an imaging lens onto a set of 75 mm-diameter microchannel plates (MCP) coupled with a phosphor screen. Various extraction voltages were used, depending on the kinetic energies of the electrons. A low extraction voltage of 300 V was used for all the resonant and nonresonant images to detect slow electrons for higher spectral resolution, while a high extraction voltage of 1000 V was used for high-photon energy images, and 1560 V was used for the resonant two-photon detachment to detect very fast photoelectrons. PE images were collected with a charge-coupled device camera and inverse-Abel-transformed using pBasex³⁸ and BASEX.³⁹ The PE spectra were calibrated with the known spectra of Au^- at different photon energies. The electron kinetic energy (KE) resolution achieved was 3.8 cm^{-1} for electrons with 55 cm^{-1} KE and about 1.5% ($\Delta KE/KE$) for electrons above 1 eV KE in the current experiment.²¹

The molecular orbitals of the triazolide anion (Figure S1) and the dipole moment of the triazolyl radical were calculated at the B3LYP/6-311++G** level of theory using Gaussian 09.⁴⁰ The energetic order of the molecular orbitals and the excited states shown in Figure S1 are based on previous *ab initio* results.¹³

3. RESULTS

3.1. Non-resonant PE Spectra of Triazolide. Figure 1 presents the non-resonant PE spectra of triazolide at two different photon energies. Figure 1a is taken near the detachment threshold, yielding a high-resolution 0_0^0 transition with a full width at half maximum of 14 cm^{-1} and an accurate electron affinity (EA) of $3.4463 \pm 0.0009\text{ eV}$ ($27,796 \pm 7\text{ cm}^{-1}$) for the triazolyl radical. The spectrum in Figure 1b at 336.15 nm (3.6884 eV) represents detachment from the ground state of triazolide (1A_1) to a broader Franck–Condon (FC) region of the triazolyl radical ground state (2B_1), revealing 18 vibronic features (labeled from A to R). Another non-resonant PE spectrum at a slightly higher photon energy of 333.95 nm (3.7127 eV) is given in Figure S2, revealing two additional vibronic features (S and T). The binding energies of all the observed vibronic peaks are given in Table S1, along with the spectral assignments and comparison with the PD spectrum (*vide infra*).

3.2. PDS and the DBS of Triazolide. Our calculation at the B3LYP level gave a dipole moment of 4.03 D for triazolyl, suggesting that the triazolide anion should have a DBS as an electronically excited state below the detachment threshold.³⁶

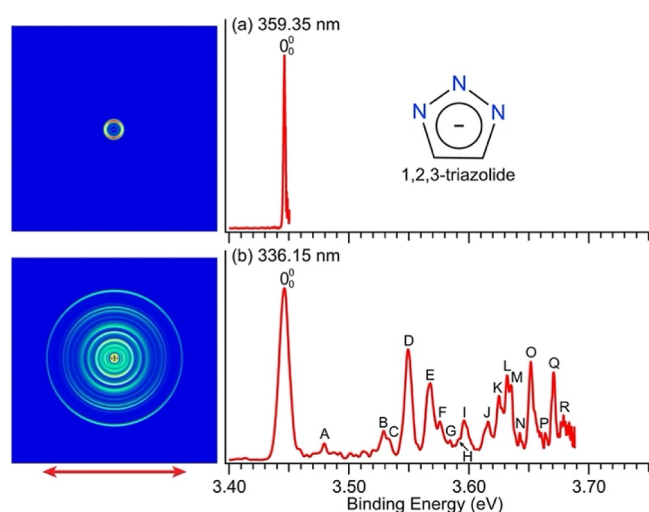


Figure 1. PE images and spectra of triazolide at (a) 359.35 nm ($27,828\text{ cm}^{-1}$, 3.4502 eV) and (b) 336.15 nm ($29,749\text{ cm}^{-1}$, 3.6884 eV). The resolved vibrational peaks are labeled with letters. The double arrow below the images indicates the laser polarization direction. The inset in (a) shows the molecular structure of 1,2,3-triazolide.

To search for the DBS, we performed PDS by monitoring the total electron yield as a function of wavelength across the detachment threshold, as shown in Figure 2 in the energy range from $27,450\text{ cm}^{-1}$ (3.4034 eV) to $29,965\text{ cm}^{-1}$ (3.7152 eV). Electron signals appeared promptly at the detachment threshold of $27,796\text{ cm}^{-1}$ (arrow in Figure 2), indicating an *s*-partial wave for the outgoing electron according to the Wigner threshold law.⁴¹ Detachment of the π HOMO of triazolide (Figure S1b) should give rise to photoelectrons of (*s* + *d*)-wave characters. Clearly, the *s*-partial wave dominates near the threshold. The PDS was conducted with a scan step of 0.1 nm. For all the observed peaks, additional PDS data were taken at a step size of 0.01 nm in order to measure the excitation energies

more accurately. The baseline above threshold represents the non-resonant photodetachment cross-sections. The sharp peaks indicate the existence of a DBS, as a result of resonant excitation to specific vibrational levels (*i.e.*, vibrational Feshbach resonances) of the DBS, followed by autodetachment.^{42–44}

The extraction voltage on the VMI lens was first set at 1000 V during the PDS, and no resonant peak was observed below the threshold for the zero-point level of the DBS, as shown in Figure S3. However, when the extraction voltage was increased to 1560 V, a weak below-threshold peak, labeled as peak 0, was observed at $27,624\text{ cm}^{-1}$ (3.4249 eV), as shown in Figure 2. This weak peak should correspond to the zero-point level of the DBS. The binding energy of the DBS, defined as the energy separation between the detachment threshold and the zero-point level of the DBS, was measured to be $172 \pm 7\text{ cm}^{-1}$ ($0.0213 \pm 0.0009\text{ eV}$). The observation of the bound zero-point level was due to a two-photon process, resulting in photoelectrons with much higher kinetic energies, so that a much higher extraction voltage was required to detect the fast electrons. The wavelengths and photon energies of the 32 observed DBS vibrational peaks are given in Table S2.

3.3. R2PD PES via the Zero-point Level of the DBS. By tuning the detachment laser to the wavelength of the bound zero-point level of the DBS and dispersing the electron kinetic energies, we obtained a single-color resonant two-photon detachment (R2PD) PE image and spectrum, as shown in Figure 3. Two peaks are observed: a low-binding energy feature labeled as “DBS” and a high-binding energy feature labeled as “ α ”. The peak labeled as “DBS” comes from the expected R2PD process, in which the first photon excites triazolide to the zero-point level of the DBS, followed by detachment of the dipole-bound electron by the second photon within the same laser pulse ($\sim 5\text{ ns}$). The binding energy measured for the DBS from the R2PD PE spectrum is $0.060 \pm 0.042\text{ eV}$ ($480 \pm 340\text{ cm}^{-1}$), which is consistent with the measurement from the PDS, albeit much less accurate due to the limited spectral resolution. The PE image in Figure 3 for

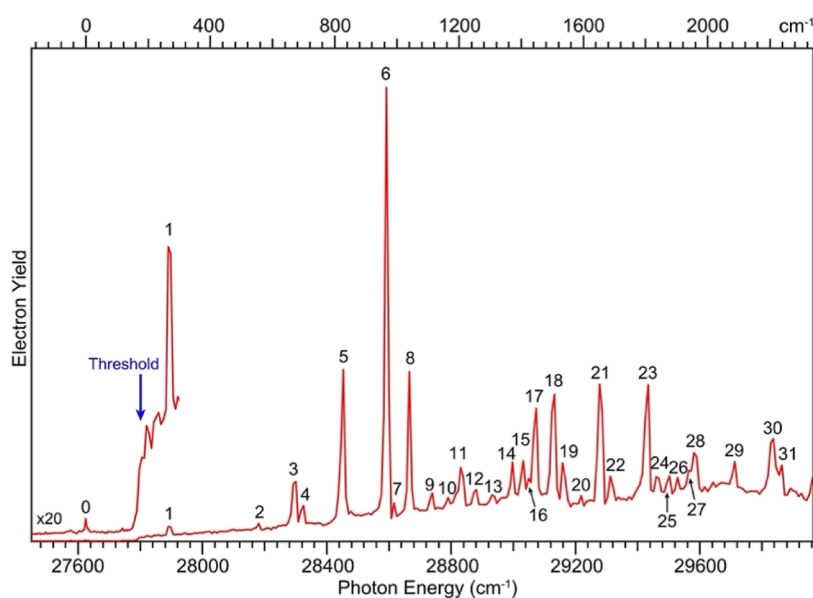


Figure 2. PD spectrum of triazolide from $27,450$ to $29,965\text{ cm}^{-1}$. The spectrum above threshold was taken with an extraction voltage of 300 V, and the spectrum below threshold was taken with an extraction voltage of 1560 V. The arrow at $27,796\text{ cm}^{-1}$ indicates the detachment threshold. The observed DBS vibrational peaks are labeled from 0 to 31.

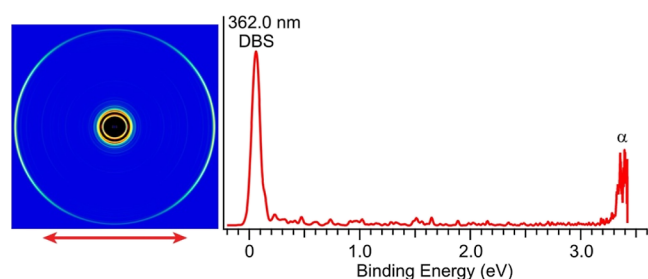


Figure 3. R2PD PE image and spectrum of triazolide at the detachment wavelength (362.00 nm) corresponding to peak 0 in Figure 2.

the “DBS” peak displays a distinct p -wave angular distribution with a β value of 1.1, consistent with the s -like dipole-bound orbital. For a pure atomic s orbital, the β value is 2.⁴⁵

3.4. Resonant PE Spectra of Triazolide. Tuning the detachment laser to each of the vibrational Feshbach resonances in Figure 2 and measuring the PE kinetic energies result in 31 resonantly-enhanced PE spectra. Resonant PE spectra *via* DBSs were first observed for the phenoxide anion and were found to be mode-selective⁴⁶ and obey the $\Delta v = -1$ propensity rule.^{47,48} Thus, resonant PES is highly non-Franck-Condon and yields much richer spectroscopic information than non-resonant PES.²⁷ The resonant PE spectra for peaks 1–10, 16, and 27 are shown in Figure 4. The remaining 19 resonant PE spectra are given in Figures S4 and S5. On comparing with the non-resonant PE spectra in Figures 1b and S2, we observed that one or more vibrational peaks were enhanced (labeled in bold face) in the resonant PE spectra and new peaks (labeled in lowercase letters) that were not present in the non-resonant PE spectra. Due to the high density of vibrational levels at higher excitation energies, overlapping vibrational levels could be excited simultaneously, producing relatively complicated resonant PE spectra. Many of the vibronic peaks observed in the non-resonant PE spectra are observed more prominently in the resonant PE spectra and at higher spectral resolution. The vibronic peak positions observed in all the resonant and nonresonant spectra, with their binding energies in both eV and cm^{-1} , shift relative to the 0_0^0 peak, and their assignments are summarized in Table S1.

4. DISCUSSION

4.1. Non-resonant PE Spectra of Triazolide and Strong Nonadiabatic Interactions. The non-resonant PE spectrum taken at 336.15 nm (Figure 1b) and 333.95 nm (Figure S2) is similar to the 335 nm spectrum by Lineberger and co-workers,⁷ who reported an EA of 3.447 ± 0.004 eV for triazolyl, consistent with the current value of 3.4463 ± 0.0009 eV ($27,796 \pm 7$ cm^{-1}). In the same spectral range, they were able to resolve 10 vibronic peaks above the 0_0^0 transition *vs* 20 in the current data (A–T in Figure S2). The current PE images also reveal angular distributions of $s + d$ characters, in accordance with the π -type HOMO of triazolide (Figure S1b). Vibrational features in non-resonant PES are usually assigned by comparison with FC simulations.^{4–6} However, no assignments of the vibrational peaks were possible in the previous PES study⁷ because of strong nonadiabatic effects. Subsequently, Yarkony and co-workers carried out a vibronic coupling study to simulate the PE spectrum of triazolide.¹³ They were able to reproduce the main PES features by considering vibronic couplings between the ground state (2B_1)

of triazolyl with its three low-lying excited states (2A_1 , 2A_2 , and 2B_2), which are close in energy (Figure S1a). In addition to the vibrational hot bands present in the PE spectrum by Lineberger and co-workers, the simulation also suggested many more unresolved vibronic features.

Ortiz and co-workers investigated the electronic structure of triazolide and calculated its detachment energies using several theoretical methods.¹⁴ At their highest level of theory (P3+), they predicted a VDE of 3.82 eV from the HOMO (b_1), resulting in the 2B_1 ground state of triazolyl, compared to the experimental value of 3.4463 eV. Their calculated VDEs for the next three MOs were well-separated from those of the HOMO but were close to each other: 4.40 eV from the a_2 orbital (2A_2 final state), 4.45 eV from the a_1 orbital (2A_1), and 4.47 eV from the b_2 orbital (2B_2). The order of the 2A_2 and 2A_1 states by Ortiz and co-workers¹⁴ was reversed from that by Yarkony and co-workers,¹³ which is adopted in Figure S1a. In any case, the previous theoretical results suggested that the first three excited states of triazolyl are close in energy and should be accessible at our detachment energy of 266 nm (4.661 eV), as shown in Figure 5. Due to the lower spectral resolution for high-KE electrons, the fine vibronic features resolved for the ground electronic state (2B_1) of triazolyl in the lower photon energy spectra up to 3.7 eV (Figures 1b and S2) are all smeared out. It is notable that continuous signals are observed in Figure 5 beyond 3.9 eV in the spectral range where the three excited states (2A_1 , 2A_2 , and 2B_2) of triazolyl are expected to appear. No fine vibronic features are resolved or attributable to any electronic states. This observation is consistent with theoretical predictions that the three excited states are close in energy and most importantly the strong nonadiabatic couplings exist among the first four electronic states,¹³ resulting in the unresolvable vibronic features.

4.2. Comparison of the Non-resonant PE Spectra with the PD Spectrum. As reported in our previous studies,²⁷ the PD spectrum of the DBS mirrors the non-resonant PE spectrum of the same anion because the diffuse dipole-bound electron has a little effect on the structure of the neutral core. The PD spectrum of triazolide is compared with its non-resonant PE spectrum at 336.15 nm in Figure 6 on the same energy scale, by aligning the 0_0^0 transition in the PE spectrum with peak 0 of the PD spectrum (the zero-point level of the DBS). The similarity between the PE spectrum and the PD spectrum can be readily seen, except for the higher resolution and the anomalously high intensities of peaks 6 and 8 for the latter. As also given in Table S1, every observed peak in the PE spectrum has a corresponding transition in the PD spectrum, except for the weak peak P. There are a few weak resonances in the PD spectrum, that is, peaks 2, 7, 12, 13, 15, 16, 22, 24, 26, and 27, that do not have corresponding transitions in the PE spectrum. These additional resonances observed due to the higher sensitivity of PDS can yield more vibrational information about the neutral radical. The similarity between the PE spectrum and the PD spectrum of triazolide confirms again that the diffuse dipole-bound electron has a very little effect on the structure of the neutral core in the DBS. More importantly, the resonant PES allows the assignments of the Feshbach resonances in the PD spectrum based on the $\Delta v = -1$ propensity rule, in addition to yielding new vibrational information. In turn, the one-to-one correspondence allows us to assign the vibronic transitions in the non-resonant PE spectra of triazolyl, which were not possible previously.⁷

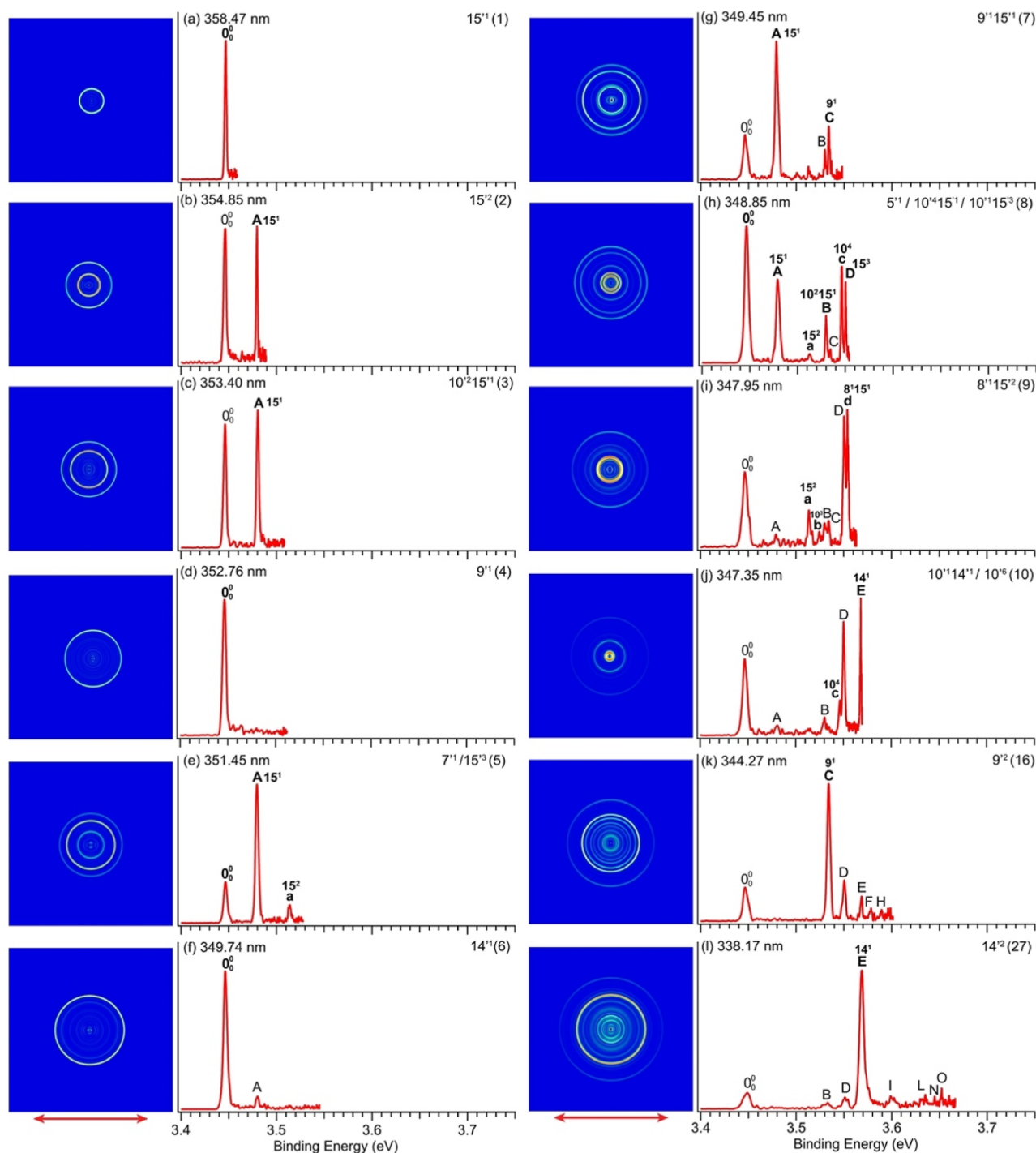


Figure 4. Selected resonant PE images and spectra of triazolide at (a) 358.47 nm ($27,896\text{ cm}^{-1}$, 3.4587 eV), (b) 354.85 nm ($28,181\text{ cm}^{-1}$, 3.4940 eV), (c) 353.40 nm ($28,297\text{ cm}^{-1}$, 3.5083 eV), (d) 352.76 nm ($28,348\text{ cm}^{-1}$, 3.5147 eV), (e) 351.45 nm ($28,454\text{ cm}^{-1}$, 3.5278 eV), (f) 349.74 nm ($28,593\text{ cm}^{-1}$, 3.5450 eV), (g) 349.45 nm ($28,616\text{ cm}^{-1}$, 3.5480 eV), (h) 348.85 nm ($28,666\text{ cm}^{-1}$, 3.5541 eV), (i) 347.95 nm ($28,740\text{ cm}^{-1}$, 3.5633 eV), (j) 347.35 nm ($28,789\text{ cm}^{-1}$, 3.5694 eV), (k) 344.27 nm ($29,047\text{ cm}^{-1}$, 3.6014 eV), and (l) 338.17 nm ($29,571\text{ cm}^{-1}$, 3.6663 eV). The numbers in the parentheses are the peak labels from the PD spectrum (Figure 2). The wavelengths and assignments are also given. The double arrows below the images indicate the laser polarization direction. The enhanced peaks are indicated by boldface. The prime ' is used to designate vibrational levels of the DBS.

Figure 6 also vividly illustrates that the vibrational frequencies of the triazolyl radical are the same as those in the DBS due to the negligible perturbation of the diffuse dipole-bound electron on the structure of the neutral core.²⁷ Thus, we can use the computed harmonic vibrational frequencies of the ground state of triazolyl reported by

Yarkony and co-workers¹³ to assist the assignments of the DBS vibrational peaks in the PD spectrum. The vibrational modes and their computed harmonic frequencies for triazolyl are given in Figure S6.

4.3. R2PD PES via the Zero-point Level of the DBS.

The peak labeled as the “DBS” on the low-binding energy side

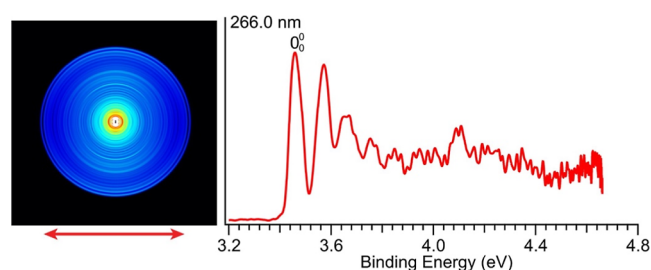


Figure 5. Photoelectron image and spectrum of triazolide at 266.0 nm (4.661 eV). The double arrows below the images indicate the laser polarization direction.

in the R2PD PE spectrum (Figure 3) is due to excitation of the anion to the zero-point level of the DBS by the first photon and subsequent detachment of the dipole-bound electron from the zero-point level by a second photon (single-color) within the same laser pulse (~ 5 ns), giving rise to a fast electron with a kinetic energy very close to the photon energy. The first single-color R2PD PE spectrum from a DBS was observed for the phenoxide anion.⁴⁶ R2PD PE spectra from DBSs probe the nature of the dipole-bound states and are similar to PE spectra of ground-state dipole-bound anions formed by Rydberg electron transfer,⁴⁹ except that in the R2PD case, the dipole-bound anion is prepared by photoexcitation of a valence-bound anion.

In almost all our previous single-color R2PD PE spectra, we observed strong high binding energy features due to fast relaxation from the bound DBS levels to either low-lying electronically or vibrationally excited states of the anion, followed by detachment by the second photon within the same laser pulse.^{50–52} The weak high binding energy feature labeled as “ α ” in the current R2PD spectrum (Figure 3) could be due to vibrationally or rotationally excited states of the triazolide anion as a result of fast relaxation from the DBS. However, this was not the case because such low-kinetic energy electrons were not observed when a lower extraction voltage on the

imaging lens was used, as illustrated in Figure S3, suggesting that the weak “ α ” feature was due to background noises. It should be pointed out that the R2PD signal shown in Figure 3 was extremely weak. The spectrum shown in Figure 3 was averaged for more than 324,000 laser shots (>9 h). Thus, the few electron counts corresponding to the weak feature denoted by “ α ” were likely due to noises, such as secondary electrons from the parent ions scattered off the surfaces around the interaction zone. Such noises would be negligible under typical experimental conditions, where single-photon detachment cross-sections are much larger than the R2PD signals. Thus, the lack of electron signals due to relaxation processes from the DBS suggested that the bound zero-point level of the DBS in triazolide is long-lived, that is, longer than the 5 ns detachment laser pulse. This long-lived DBS (>5 ns) is rather rare because we have observed relaxation effects in all the previous R2PD PE spectra of bound DBS levels.^{50–52} This observation suggests that the coupling of the DBS with the ground state of the triazolide anion is weak.

4.4. Resonant PES via the Feshbach Resonances of the DBS. Two detachment processes contribute to the resonant PE spectra: (1) the non-resonant detachment process corresponding to the rising baseline above the threshold in the PD spectrum (Figure 2) and (2) the resonantly enhanced vibrational autodetachment, which is a two-step process. The first step involves resonant excitation of the anion to a specific vibrational Feshbach resonance of the DBS, followed by vibrationally induced autodetachment, in which the vibrational energy is coupled to the dipole-bound electron. Autodetachment from vibrational levels of the DBS follows the $\Delta v = -1$ propensity rule under the harmonic approximation,^{47,48} which means that only one vibrational quantum can be coupled to the dipole-bound electron during autodetachment. The $\Delta v = -1$ propensity rule is a direct manifestation of the similarity between the structures of the DBS and the neutral. For example, if the triazolide anion is excited to the DBS vibrational level $\nu_x'^n$ (the n th quantum of the ν_x' mode, the prime ' refers to the DBS modes), autodetachment will lead to

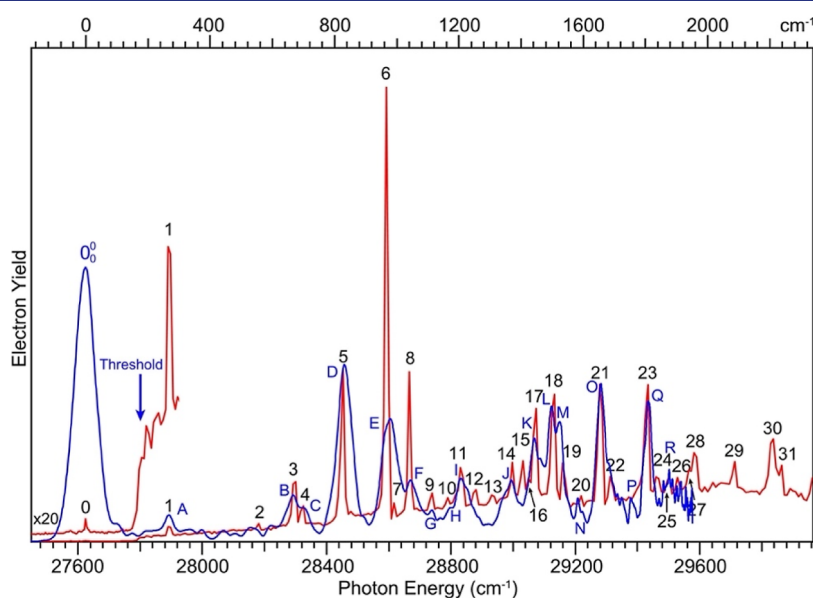


Figure 6. Comparison of the non-resonant PE spectrum (blue) at 336.15 nm (Figure 1b) with the photodetachment spectrum (red) (Figure 2). The non-resonant PE spectrum is shifted to line up with the photodetachment spectrum. The labels for the PE and PD spectra are retained. See Table S1 for the one-to-one correspondence of the PE and PD spectral features.

the $(n - 1)$ th level of the same vibrational mode in the triazolyl radical (ν_x^{n-1}), which will be enhanced in the resonant PE spectrum. For autodetachment from a combinational level ($\nu_x^n \nu_y^m \dots$) of the DBS, the final neutral state can be either $\nu_x^{n-1} \nu_y^m \dots$ or $\nu_x^n \nu_y^{m-1} \dots$, producing multiple enhanced vibrational peaks in the resonant PE spectra. Violation of the $\Delta v = -1$ propensity rule can happen as a result of anharmonicity⁴⁷ and has been observed often for low-frequency bending modes. As will be seen below, the two lowest frequency modes of triazolyl, mode ν_{10} with b_1 symmetry and mode ν_{15} with b_2 symmetry, appear in many of the observed Feshbach resonances, and violation of the $\Delta v = -1$ propensity rule is observed in some resonant PE spectra involving these two modes because of their strong anharmonic behaviors.^{12,13} Furthermore, some of the observed resonant peaks in the PD spectrum may contain excitations to near-degenerate or overlapping vibrational levels, especially at high excitation energies, giving rise to more complicated resonant PE spectra.

The resonant PES allows the Feshbach resonances to be assigned using the $\Delta v = -1$ propensity rule. This is particularly important for the triazolide anion because its non-resonant PE spectrum was not possible to be assigned previously due to strong vibronic couplings.⁷ As shown in Figure 6, the one-to-one correspondence between the PE and PD spectra allows us to assign the PES features readily, if the vibrational peaks of the DBS in the PD spectrum can be assigned using the resonant PE spectra shown in Figures 4 and S4 and S5.

4.5. Resonant PES at Low Excitation Energies of the DBS. Figure 4a is taken at the weak resonant peak 1 at 358.47 nm in the PD spectrum (Figure 2). Since only the 0–0 transition was observed, peak 1 must correspond to a fundamental excitation of a specific mode of the DBS. The energy separation between peak 1 and peak 0 is 272 cm^{-1} (Table S2), which is close to the computed harmonic frequency of the ν_{15} mode (304.1 cm^{-1}) of triazolyl by Yarkony and co-workers.¹³ Thus, peak 1 should be due to the fundamental excitation of the DBS mode ν_{15}' (Figure S6). Figure 6 and Table S1 show that peak 1 corresponds to peak A in the non-resonant PE spectrum. Thus, peak A should be due to the $v = 1$ level of mode ν_{15} of triazolyl (15^1). This weak peak was not observed in the previous PES study by Lineberger and co-workers⁷ but was predicted by the vibronic coupling calculations of Yarkony and co-workers.¹³ Peak A is significantly enhanced in the resonant PE spectrum shown in Figure 4b taken at the resonant peak 2 (Figure 2) due to autodetachment from the $\nu_{15}'^2$ level of the DBS following the $\Delta v = -1$ propensity rule. The corresponding $\nu_{15}'^2$ peak was not observed in the non-resonant PE spectrum (Figure 6) due to its negligible FC factor. Figure 4b shows a vivid demonstration of how a weak transition in non-resonant PES can be lighted up in the rPES. Peak A is also enhanced in Figure 4c,e,g,h. Figure 4c taken at resonant peak 3 is due to excitation to a combinational vibrational level, $\nu_{10}'^2 \nu_{15}'^1$, of the DBS. Coupling of two quanta of the ν_{10}' mode with the dipole-bound electron leads to the enhanced $\nu_{15}'^1$ final state in violation of the $\Delta v = -1$ propensity rule. It seems that the ν_{15}' mode has weak coupling with the dipole-bound electron because the expected $\nu_{10}'^2$ final state is not observed in Figure 4c. Such mode-selective vibrational autodetachment in DBS was first observed for the phenoxide anion⁴⁶ and has been recently probed in a pump–probe experiment.⁵³ Peak 3 corresponds to peak B in the non-resonant PE spectrum

(Figure 6 and Table S1); thus, peak B should be due the combinational vibrational level, $\nu_{10}'^2 \nu_{15}'^1$, of triazolyl.

Figure 4e taken at resonant peak 5 also produces the $\nu_{15}'^2$ final state, suggesting the excitation of the $\nu_{15}'^3$ Feshbach resonance. The strong peak A (15^1) indicates the coupling of two quanta of the ν_{15}' mode with the dipole-bound electron. Peak 5 is a strong resonant peak, which also contains an overlapping vibrational excitation of $\nu_7'^1$, resulting in an enhanced 0_0^0 peak. Although it is difficult to assess the enhancement of the 0_0^0 peak from the relative peak intensity, the more isotropic angular distribution in the PE image suggests strong contributions to the 0_0^0 transition from autodetachment. Considering the fact that the $\nu_{15}'^2$ transition is negligible in the non-resonant PE spectra, peak D—the strongest vibronic transition above the 0–0 level in Figure 1b—should be mainly due to the $\nu_7'^1$ transition, instead of $\nu_{15}'^3$. The enhancement of peak A in Figure 4g taken at peak 7 was due to the excitation of the combinational level $\nu_9'^1 \nu_{15}'^1$ of the DBS, which also yields an enhancement for peak C (9^1). Peak 7 is a very weak transition, but the enhancement of peaks A and C is quite pronounced in Figure 4g.

Figure 4d taken at peak 4 displays an enhanced 0_0^0 peak, suggesting the excitation of the $\nu_9'^1$ level of the DBS. The separation of peak 4 from peak 0 is 724 cm^{-1} (Table S2), which is close to the computed frequency for the ν_9 mode (Figure S6).¹³ Thus, peak C in Figure 1b can be safely assigned to the 9^1 final state (Figure 6 and Table S1). Figure 4k taken at peak 16 displays a single enhanced peak C (9^1) due to the excitation of the $\nu_9'^2$ level of the DBS. Similarly, Figure 4f,l taken at peaks 6 and 27 is due to excitations to the $\nu_{14}'^1$ and $\nu_{14}'^2$ levels of the DBS, respectively, displaying strong enhancement of the 0_0^0 peak and peak E (14^1), according to the $\Delta v = -1$ propensity rule. Peak 6 ($\nu_{14}'^1$), the most intense peak in the photodetachment spectrum (Figure 2), is anomalous because the corresponding vibrational peak (peak E due to $\nu_{14}'^1$) in the non-resonant PE spectra does not have the strongest FC factor. The anomalous intensity of peak 6 is also manifested by the relatively weak overtone excitation of the ν_{14}' mode (peak 27), whereas the corresponding 14^2 transition is negligible in the non-resonant PE spectra. The anomalous intensity of peak 6 suggests that it may contain overlapping vibrational transitions that have long autodetachment lifetimes and are not observed in the resonant PE spectrum. One such possibility is the $\nu_{10}'^2 \nu_{15}'^2$ combinational DBS level, which is expected to be close to peak 6. In fact, the mere observation of peak A (very weak in the non-resonant PE spectrum) in Figure 4f suggests that it must be resonantly enhanced, considering the fact that the 0_0^0 transition is strongly enhanced. This observation provides support for an overlapping vibrational level in peak 6. Even though the resonant peak 16 ($\nu_9'^2$) and peak 27 ($\nu_{14}'^2$) are extremely weak transitions in the PD spectrum (Figure 2), the enhancement shown in the resonant PE spectra (peak C in Figure 4k and peak E in Figure 4l) is very prominent, providing unambiguous information for the spectral assignments. Therefore, peaks C and E could also be readily assigned to ν_9^1 and ν_{14}^1 . The overtone transitions (ν_9^2 and ν_{14}^2) of these two modes are negligible in the non-resonant PE spectra, even though the corresponding transitions are observed in the PD spectrum (peak 16 and peak 27 in Figure 2).

The resonant PE spectrum shown in Figure 4h taken at peak 8 (Figure 2) is somewhat complicated, indicating that peak 8 consists of overlapping vibrational levels of the DBS. The

Table 1. Observed Vibrational Modes and Their Fundamental Frequencies for the Ground State of Triazolyl Radical From the Current Work, in Comparison With the Calculated Harmonic Frequencies^a

vibrational mode	symmetry	ω (exp.) (cm ⁻¹)	ω (theo.) (cm ⁻¹) ^a
ν_{15}	b ₂	273(4)	304.1
ν_{14}	b ₂	972(3)	992.3
ν_{13}	b ₂	1202(7)	1217.9
ν_{12}^b	b ₂	1595(3)	1553.3
ν_{10}	b ₁	197(4)	204.2
ν_9	b ₁	719(5)	785.5
ν_8	a ₂	575(5)	576.5
ν_7	a ₂	831(3)	859.3
ν_6	a ₁	942(6)	933.6
ν_5	a ₁	1040(3)	1052.0
ν_3	a ₁	1300(5)	1344.6
ν_2^b	a ₁	1595(3)	1558.0

^aThe theoretical frequencies are from ref 13. ^bThese two modes cannot be distinguished from the current experiment.

5. CONCLUSIONS

In conclusion, we report a complete unraveling of the complicated nonadiabatic vibronic features of the triazolyl radical, using high-resolution photoelectron imaging, photo-detachment spectroscopy, and resonant photoelectron spectroscopy of cryogenically cooled triazolide anions. The electron affinity of the triazolyl radical is measured accurately to be 3.4463 ± 0.0009 eV ($27,796 \pm 7$ cm⁻¹). A DBS is observed for triazolide at 172 ± 7 cm⁻¹ below the detachment threshold. Single-color resonant two-photon PES suggests that the DBS is long-lived (>5 ns). Thirty-one above-threshold resonances of the DBSs are observed in the photodetachment spectrum, which are used to obtain 31 resonantly enhanced photoelectron spectra *via* vibrational autodetachment. Twenty-eight vibronic levels are observed for the ground state of triazolyl and are assigned by comparing the non-resonant PE spectra with the photodetachment spectrum assisted with the resonant PE spectra. A total of 12 fundamental vibrational frequencies are measured for the triazolyl radical by combining the photodetachment spectroscopy and resonant and non-resonant photoelectron spectroscopy. The rich vibronic information would be valuable to further understand the nonadiabatic vibronic couplings in the triazolyl radical and provide important experimental references for further theoretical investigations. This study demonstrates again that the combination of photodetachment spectroscopy and resonant photoelectron spectroscopy is a powerful tool to obtain vibrational information and unravel complex vibronic structures for dipolar neutral radical species *via* vibrational autodetachment from DBSs.

■ ASSOCIATED CONTENT

Supporting Information

The Supporting Information is available free of charge at <https://pubs.acs.org/doi/10.1021/jacs.2c07167>.

Valence molecular orbitals of triazolide and low-lying electronic states of triazolyl; additional non-resonant photoelectron spectrum, photodetachment spectrum, and resonant photoelectron spectra; normal modes of vibration of triazolyl; additional energy level diagrams of autodetachment from the DBS; detailed binding

energies and assignments of all the resolved vibronic levels of triazolyl; and detailed photon energies and assignments of all the observed vibrational Feshbach resonances (PDF)

■ AUTHOR INFORMATION

Corresponding Authors

Dao-Fu Yuan – Department of Chemistry, Brown University, Providence, Rhode Island 02912, United States;

orcid.org/0000-0001-8461-6889; Email: daofu_yuan@brown.edu

Lai-Sheng Wang – Department of Chemistry, Brown University, Providence, Rhode Island 02912, United States;

orcid.org/0000-0003-1816-5738; Email: lai-sheng_wang@brown.edu

Author

Yue-Rou Zhang – Department of Chemistry, Brown University, Providence, Rhode Island 02912, United States

Complete contact information is available at:

<https://pubs.acs.org/10.1021/jacs.2c07167>

Notes

The authors declare no competing financial interest.

■ ACKNOWLEDGMENTS

This work was supported by the U.S. Department of Energy, Office of Basic Energy Sciences, Chemical Sciences, Geosciences, and Biosciences Division under grant DE-SC0018679. The calculations were performed using resources from the Center for Computation and Visualization (CCV) of Brown University.

■ REFERENCES

- (1) *Conical Intersections: Theory, Computation and Experiment*; Domcke, W., Yarkony, D. R., Koppel, H., Eds.; World Scientific: London, 2011; Vol. 17.
- (2) Domcke, W.; Yarkony, D. R. Role of Conical Intersections in Molecular Spectroscopy and Photoinduced Chemical Dynamics. *Annu. Rev. Phys. Chem.* **2012**, *63*, 325–352.
- (3) Schuurman, M. S.; Stolow, A. Dynamics at Conical Intersections. *Annu. Rev. Phys. Chem.* **2018**, *69*, 427–450.
- (4) Gianola, A. J.; Ichino, T.; Hoenigman, R. L.; Kato, S.; Bierbaum, V. M.; Lineberger, W. C. Thermochemistry and Electronic Structure of the Pyrrolyl Radical. *J. Phys. Chem. A* **2004**, *108*, 10326–10335.
- (5) Gianola, A. J.; Ichino, T.; Hoenigman, R. L.; Kato, S.; Bierbaum, V. M.; Lineberger, W. C. Photoelectron Spectra and Ion Chemistry of Imidazolide. *J. Phys. Chem. A* **2005**, *109*, 11504–11514.
- (6) Gianola, A. J.; Ichino, T.; Kato, S.; Bierbaum, V. M.; Lineberger, W. C. Thermochemical Studies of Pyrazolide. *J. Phys. Chem. A* **2006**, *110*, 8457–8466.
- (7) Ichino, T.; Kato, S.; Wren, S. W.; Bierbaum, V. M.; Lineberger, W. C. Ion Chemistry of 1H-1,2,3-Triazole. 2. Photoelectron Spectrum of the Iminodiazomethyl Anion and Collision Induced Dissociation of the 1,2,3-Triazolide Ion. *J. Phys. Chem. A* **2008**, *112*, 9723–9730.
- (8) Ichino, T.; Gianola, A. J.; Lineberger, W. C.; Stanton, J. F. Nonadiabatic Effects in the Photoelectron Spectrum of the Pyrazolide-*d*₃ Anion: Three-State Interactions in the Pyrazolyl-*d*₃ Radical. *J. Chem. Phys.* **2006**, *125*, 084312.
- (9) Motzke, A.; Lan, Z.; Woywod, C.; Domcke, W. Simulation of the Photodetachment Spectrum of the Pyrrolyl Anion. *Chem. Phys.* **2006**, *329*, 50–64.
- (10) Schuurman, M. S.; Yarkony, D. R. A Simulation of the Photoelectron Spectrum of Pyrazolide. *J. Chem. Phys.* **2008**, *129*, 064304.

- (11) Zhu, X.; Yarkony, D. R. The Photoelectron Spectrum of Pyrrolide: Nonadiabatic Effects due to Conical Intersections. *J. Phys. Chem. C* **2010**, *114*, 5312–5320.
- (12) Dillon, J.; Yarkony, D. R.; Schuurman, M. S. On the Construction of Quasidiabatic State Representations of Bound Adiabatic State Potential Energy Surfaces Coupled by Accidental Conical Intersections: Incorporation of Higher Order Terms. *J. Chem. Phys.* **2011**, *134*, 044101.
- (13) Dillon, J.; Yarkony, D. R.; Schuurman, M. S. On the Simulation of Photoelectron Spectra Complicated by Conical Intersections: Higher-Order Effects and Hot Bands in the Photoelectron Spectrum of Triazolide (CH)₂N₃⁻. *J. Chem. Phys.* **2011**, *134*, 184314.
- (14) Melin, J.; Mishra, M. K.; Ortiz, J. V. Electronic Structure Analysis and Electron Detachment Energies of Polynitrogen Pentagonal Aromatic Anions. *J. Phys. Chem. A* **2006**, *110*, 12231–12235.
- (15) Applegate, B. E.; Miller, T. A.; Barckholtz, T. A. The Jahn-Teller and Related Effects in the Cyclopentadienyl Radical. I. The Ab Initio Calculations of Spectroscopically Observable Parameters. *J. Chem. Phys.* **2001**, *114*, 4855–4868.
- (16) Applegate, B. E.; Bezzant, A. J.; Miller, T. A. The Jahn-Teller and Related Effects in the Cyclopentadienyl Radical. II. Vibrational Analysis of the A²A''₂ – X²E''₁ Electronic Transition. *J. Chem. Phys.* **2001**, *114*, 4869–4882.
- (17) Ichino, T.; Wren, S. W.; Vogelhuber, K. M.; Gianola, A. J.; Lineberger, W. C.; Stanton, J. F. The Vibronic Level Structure of the Cyclopentadienyl Radical. *J. Chem. Phys.* **2008**, *129*, 084310.
- (18) Callis, P. R. Electronic States and Luminescence of Nucleic Acid Systems. *Annu. Rev. Phys. Chem.* **1983**, *34*, 329–357.
- (19) Creed, D. The Photophysics and Photochemistry of the Near-UV Absorbing Amino Acids – I. Tryptophan and Its Simple Derivatives. *Photochem. Photobiol.* **1984**, *39*, 537–562.
- (20) Crespo-Hernández, C. C.; Cohen, B.; Hare, P. M.; Kohler, B. Ultrafast Excited-State Dynamics in Nucleic Acids. *Chem. Rev.* **2004**, *104*, 1977–2020.
- (21) Wang, L. S. Perspective: Electrospray Photoelectron Spectroscopy: From Multiply-Charged Anions to Ultracold Anions. *J. Chem. Phys.* **2015**, *143*, 040901.
- (22) Wang, X. B.; Woo, H. K.; Wang, L. S. Vibrational Cooling in a Cold Ion Trap: Vibrationally Resolved Photoelectron Spectroscopy of Cold C₆₀⁻ Anions. *J. Chem. Phys.* **2005**, *123*, 051106.
- (23) Waters, T.; Wang, X. B.; Wang, L. S. Electrospray Ionization Photoelectron Spectroscopy: Probing the Electronic Structure of Inorganic Metal Complexes in the Gas Phase. *Coord. Chem. Rev.* **2007**, *251*, 474–491.
- (24) Wang, X. B.; Wang, L. S. Development of a Low-Temperature Photoelectron Spectroscopy Instrument Using an Electrospray Ion Source and a Cryogenically Controlled Ion Trap. *Rev. Sci. Instrum.* **2008**, *79*, 073108.
- (25) Huang, D. L.; Dau, P. D.; Liu, H. T.; Wang, L. S. High-Resolution Photoelectron Imaging of Cold C₆₀⁻ Anions and Accurate Determination of the Electron Affinity of C₆₀. *J. Chem. Phys.* **2014**, *140*, 224315.
- (26) Zhu, G. Z.; Liu, Y.; Hashikawa, Y.; Zhang, Q. F.; Murata, Y.; Wang, L. S. Probing the Interaction between the Encapsulated Water Molecule and the Fullerene Cages in H₂O@C₆₀⁻ and H₂O@C₅₉N⁻. *Chem. Sci.* **2018**, *9*, 5666–5671.
- (27) Zhu, G. Z.; Wang, L. S. High-Resolution Photoelectron Imaging and Resonant Photoelectron Spectroscopy via Noncovalent-Bound Excited States of Cryogenically-Cooled Anions. *Chem. Sci.* **2019**, *10*, 9409–9423.
- (28) Merkt, F. Molecules in High Rydberg States. *Annu. Rev. Phys. Chem.* **1997**, *48*, 675–709.
- (29) Softley, T. P. Application of Molecular Rydberg States in Chemical Dynamics and Spectroscopy. *Int. Rev. Phys. Chem.* **2004**, *23*, 1–78.
- (30) Yuan, D. F.; Liu, Y.; Qian, C. H.; Zhang, Y. R.; Rubenstein, B. M.; Wang, L. S. Observation of a π -Type Dipole-Bound State in Molecular Anions. *Phys. Rev. Lett.* **2020**, *125*, 073003.
- (31) Yuan, D. F.; Liu, Y.; Qian, C. H.; Kocheril, G. S.; Zhang, Y. R.; Rubenstein, B. M.; Wang, L. S. Polarization of Valence Orbitals by the Intramolecular Electric Field from a Diffuse Dipole-Bound Electron. *J. Phys. Chem. Lett.* **2020**, *11*, 7914–7919.
- (32) Qian, C.-H.; Zhang, Y.-R.; Yuan, D.-F.; Wang, L.-S. Photodetachment Spectroscopy and Resonant Photoelectron Imaging of Cryogenically-Cooled 1-Pyrenolate. *J. Chem. Phys.* **2021**, *154*, 094308.
- (33) Yuan, D.-F.; Zhang, Y.-R.; Qian, C.-H.; Liu, Y.; Wang, L.-S. Probing the Dipole-Bound State in the 9-Phenanthrolate Anion by Photodetachment Spectroscopy, Resonant Two-Photon Photoelectron Imaging, and Resonant Photoelectron Spectroscopy. *J. Phys. Chem. A* **2021**, *125*, 2967–2976.
- (34) Zhang, Y.-R.; Yuan, D.-F.; Wang, L.-S. Probing the Electronic Structure and Spectroscopy of the Pyrrolyl and Imidazolyl Radicals using High Resolution Photoelectron Imaging of Cryogenically-Cooled Anions. *Phys. Chem. Chem. Phys.* **2022**, *24*, 6505–6514.
- (35) Zhang, Y. R.; Yuan, D. F.; Wang, L. S. Observation of Core-Excited Dipole-Bound States. *J. Phys. Chem. Lett.* **2022**, *13*, 2124–2129.
- (36) Qian, C. H.; Zhu, G. Z.; Wang, L. S. Probing the Critical Dipole Moment to Support Excited Dipole-Bound States in Valence-Bound Anions. *J. Phys. Chem. Lett.* **2019**, *10*, 6472–6477.
- (37) León, I.; Yang, Z.; Liu, H. T.; Wang, L. S. The Design and Construction of a High-Resolution Velocity-Map Imaging Apparatus for Photoelectron Spectroscopy Studies of Size-Selected Clusters. *Rev. Sci. Instrum.* **2014**, *85*, 083106.
- (38) Garcia, G. A.; Nahon, L.; Powis, I. Two-Dimensional Charged Particle Image Inversion Using a Polar Basis Function Expansion. *Rev. Sci. Instrum.* **2004**, *75*, 4989–4996.
- (39) Dribinski, V.; Ossadtchi, A.; Mandelshtam, V. A.; Reisler, H. Reconstruction of Abel-Transformable Images: The Gaussian Basis-Set Expansion Abel Transform Method. *Rev. Sci. Instrum.* **2002**, *73*, 2634–2642.
- (40) Frisch, M. J.; Trucks, G. W.; Schlegel, H. B.; Scuseria, G. E.; Robb, M. A.; Cheeseman, J. R.; Scalmani, G.; Barone, V.; Petersson, G. A.; Nakatsuji, H.; Li, X.; Caricato, M.; Marenich, A.; Bloino, J.; Janesko, B. G.; Gomperts, R.; Mennucci, B.; Hratchian, H. P.; Ortiz, J. V.; Izmaylov, A. F.; Sonnenberg, J. L.; Williams-Young, D.; Ding, F.; Lipparini, F.; Egidi, F.; Goings, J.; Peng, B.; Petrone, A.; Henderson, T.; Ranasinghe, D.; Zakrzewski, V. G.; Gao, J.; Rega, N.; Zheng, G.; Liang, W.; Hada, M.; Ehara, M.; Toyota, K.; Fukuda, R.; Hasegawa, J.; Ishida, M.; Nakajima, T.; Honda, Y.; Kitao, O.; Nakai, H.; Vreven, T.; Throssell, K.; Montgomery, J. A., Jr.; Peralta, J. E.; Ogliaro, F.; Bearpark, M.; Heyd, J. J.; Brothers, E.; Kudin, K. N.; Staroverov, V. N.; Keith, T.; Kobayashi, R.; Normand, J.; Raghavachari, K.; Rendell, A.; Burant, J. C.; Iyengar, S. S.; Tomasi, J.; Cossi, M.; Millam, J. M.; Klene, M.; Adamo, C.; Cammi, R.; Ochterski, J. W.; Martin, R. L.; Morokuma, K.; Farkas, O.; Foresman, J. B.; Fox, D. J. *Gaussian 09*, Revision D.01; Gaussian, Inc.: Wallingford CT, 2016.
- (41) Wigner, E. P. On the Behavior of Cross Sections Near Thresholds. *Phys. Rev.* **1948**, *73*, 1002–1009.
- (42) Jackson, R. L.; Hiberty, P. C.; Brauman, J. I. Threshold Resonances in the Electron Photodetachment Spectrum of Acetaldehyde Enolate Anion. Evidence for a Low-lying, Dipole-supported State. *J. Chem. Phys.* **1981**, *74*, 3705–3712.
- (43) Yokoyama, K.; Leach, G. W.; Kim, J. B.; Lineberger, W. C.; Boldyrev, A. I.; Gutowski, M. Autodetachment Spectroscopy and Dynamics of Vibrationally Excited Dipole-Bound States of H₂CCC⁻. *J. Chem. Phys.* **1996**, *105*, 10706–10718.
- (44) Liu, H. T.; Ning, C. G.; Huang, D. L.; Wang, L. S. Vibrational Spectroscopy of the Dehydrogenated Uracil Radical via Autodetachment of Dipole-Bound Excited States of Cold Anions. *Angew. Chem., Int. Ed.* **2014**, *53*, 2464–2468.
- (45) Cooper, J.; Zare, R. N. Angular Distribution of Photoelectrons. *J. Chem. Phys.* **1968**, *48*, 942–943.
- (46) Liu, H. T.; Ning, C. G.; Huang, D. L.; Dau, P. D.; Wang, L. S. Observation of Mode-Specific Vibrational Autodetachment from

Dipole-Bound States of Cold Anions. *Angew. Chem., Int. Ed.* **2013**, *52*, 8976–8979.

(47) Berry, R. S. Ionization of Molecules at Low Energies. *J. Chem. Phys.* **1966**, *45*, 1228–1245.

(48) Simons, J. Propensity Rules for Vibration-Induced Electron Detachment of Anions. *J. Am. Chem. Soc.* **1981**, *103*, 3971–3976.

(49) Ciborowski, S. M.; Liu, G.; Graham, J. D.; Buytendyk, A. M.; Bowen, K. H. Dipole-Bound Anions: Formed by Rydberg Electron Transfer (RET) and Studied by Velocity Map Imaging-Anion Photoelectron Spectroscopy (VMI-aPES). *Eur. Phys. J. D* **2018**, *72*, 139.

(50) Zhu, G. Z.; Cheung, L. F.; Liu, Y.; Qian, C. H.; Wang, L. S. Resonant Two-Photon Photoelectron Imaging and Intersystem Crossing from Excited Dipole-Bound States of Cold Anions. *J. Phys. Chem. Lett.* **2019**, *10*, 4339–4344.

(51) Zhang, Y.-R.; Yuan, D.-F.; Qian, C.-H.; Wang, L.-S. Observation of a Dipole-Bound Excited State in 4-Ethynylphenoxide and Comparison with the Quadrupole-Bound Excited State in the Isoelectronic 4-Cyanophenoxide. *J. Chem. Phys.* **2021**, *155*, 124305.

(52) Yuan, D.-F.; Zhang, Y.-R.; Qian, C.-H.; Wang, L.-S. Resonant Two-Photon Photoelectron Imaging and Adiabatic Detachment Processes from Bound Vibrational Levels of Dipole-Bound States. *Phys. Chem. Chem. Phys.* **2022**, *24*, 1380–1389.

(53) Kang, D. H.; An, S.; Kim, S. K. Real-Time Autodetachment Dynamics of Vibrational Feshbach Resonances in a Dipole-Bound State. *Phys. Rev. Lett.* **2020**, *125*, 093001.

(54) Huang, D. L.; Liu, H. T.; Ning, C. G.; Dau, P. D.; Wang, L. S. Resonant Photoelectron Imaging of Deprotonated Uracil Anion via Vibrational Levels of a Dipole-Bound Excited State. *Chem. Phys.* **2017**, *482*, 374–383.

Recommended by ACS

Dipole-Bound State, Photodetachment Spectroscopy, and Resonant Photoelectron Imaging of Cryogenically-Cooled 2-Cyanopyrrolide

Dao-Fu Yuan, Lai-Sheng Wang, *et al.*

SEPTEMBER 12, 2022
THE JOURNAL OF PHYSICAL CHEMISTRY A

READ 

Experimental Observation of the Resonant Doorways to Anion Chemistry: Dynamic Role of Dipole-Bound Feshbach Resonances in Dissociative Electron Attachment

Do Hyung Kang, Sang Kyu Kim, *et al.*

AUGUST 16, 2022
JOURNAL OF THE AMERICAN CHEMICAL SOCIETY

READ 

Probing the Electronic Structure and Bond Dissociation of SO₃ and SO₃⁻ Using High-Resolution Cryogenic Photoelectron Imaging

Dao-Fu Yuan, Lai-Sheng Wang, *et al.*

JULY 20, 2022
JOURNAL OF THE AMERICAN CHEMICAL SOCIETY

READ 

Observation of Transient Anions That Do Not Decay through Dissociative Electron Attachment: New Pathways for Radiosensitization

Ana I. Lozano, Gustavo García, *et al.*

JULY 27, 2022
THE JOURNAL OF PHYSICAL CHEMISTRY LETTERS

READ 

Get More Suggestions >